Received: 19 May 2025 | Revised: 28 July 2025 | Accepted: 4 August 2025

DOI: 10.1002/qj.70014

Quarterly Journal of the Royal Meteorological Society | RMetS

RESEARCH ARTICLE

Can tropical cyclones exist near the Equator?

Min Li | **Ralf Toumi**

Department of Physics, Imperial College London, London, UK

Correspondence
Min Li, Department of Physics, Imperial College London, London, UK.
Email: m.li22@imperial.ac.uk

Funding information
Natural Environmental Research Council, Grant/Award Number: NE/W009587/1; Singapore Green Finance Centre; Vodafone Foundation

Abstract

Tropical cyclones (TCs) rarely form within about 5 degrees of latitude of the Equator due to the weak Coriolis force, yet it is not clear how a weak Coriolis force would affect an already developed TC vortex. In this study, a set of Coriolis parameter (f) sensitivity experiments are applied to a well-developed TC vortex in idealized simulations by decreasing f to zero, both abruptly and gradually. The simulated TCs weaken due to the reduction of f. However, depending on the initial intensity, it can take several days for the TC to decay to a tropical storm. Both radial inflow and outflow strengthen throughout the cyclone depth, because of decreasing inertial stability and increasing agradient force associated with reduced f. This further causes a deeper inflow layer and strengthened downdrafts associated with convection in the outer rainbands. The downdraft entrainment of mid-level dry air into the deeper inflow layer stabilizes the boundary layer and suppresses deep convection, ultimately resulting in the weakening of TCs. Although TCs are not formed readily near the Equator, if they are steered there they could potentially exist long enough to cause damage.

KEYWORDS

Coriolis effect, decay, downdrafts, inflow layer depth, tropical cyclones

1 | INTRODUCTION

Tropical cyclones (TCs) are among the most destructive natural phenomena, posing significant risks to coastal regions and human life: for example, see Sparks and Toumi (2024) and Young and Hsiang (2024). The Coriolis parameter f, a fundamental aspect of geophysical flow, plays a pivotal role in TC genesis and governing the TC circulation. The Coriolis effect is a consequence of Earth's rotation. It initiates cyclonic rotation by deflecting moving air—counter-clockwise in the Northern Hemisphere and clockwise in the Southern Hemisphere. It is widely accepted that cyclones rarely form within about 5° of the Equator due to the weak Coriolis effect there (Briegel & Frank, 1997; Gray, 1968, 1979, 1985, 1998).

However, there appear to be some exceptions. One noteworthy example is Typhoon *Vamei*, which was first classified as a tropical depression at about latitude 1.5°N on December 26, 2001 over the South China Sea. It was caused by a persistent low-level cyclonic Borneo vortex and the enhancement of background cyclonic vorticity by a cold surge (Chang *et al.*, 2003). Some studies have also investigated TC formation near the Equator using idealized simulations initialized with a weak prescribed vortex, and have examined events such as Typhoon *Vamei* and Hurricane *Pali* using ECMWF analysis data (Kilroy *et al.*, 2020; Steenkamp *et al.*, 2019). The results show that cyclogenesis processes near the Equator are similar to those in higher latitudes, indicating that Earth's background rotation is not essential for TC genesis if an initial vortex is present and can be intensified by other systems.

As the Coriolis parameter, f, is directly related to planetary vorticity, it influences the TC size as an environmental factor by contributing planetary angular momentum to the TC system. Climatology studies have shown that TCs develop a larger outer size at higher latitudes, with more sufficient import of planetary angular momentum in the lower troposphere (Chan & Chan, 2013; Merrill, 1984). An analytic growth model shows that the mean latitude during growth is one of the four factors dominating the growth of the outer size, with TCs tending to grow faster at higher latitudes (Wang & Toumi, 2022). Simulation work by (Li *et al.*, 2012) confirms that not only is the outer size larger at higher latitudes, but the radius of maximum wind (RMW) is also larger. Whereas the larger RMW is attributed to higher inertial stability at higher latitudes, the outer size is determined primarily by environmental angular momentum import.

The Coriolis effect affects the intensification rate of TCs. Model simulations have shown that TCs intensify more rapidly at lower latitudes (DeMaria & Pickle, 1988; Li *et al.*, 2012; Rappin *et al.*, 2011; Smith *et al.*, 2011). Li *et al.* (2012) attributed this to stronger and deeper subgradient inflow under a lower planetary vorticity environment, which enhances boundary-layer moisture convergence and condensational heating, thereby facilitating faster TC development compared with higher planetary vorticity conditions. Smith *et al.* (2015) similarly explained that TCs at lower latitudes possess stronger inflow in the boundary layer, which induces stronger convergence of absolute angular momentum and thus more rapid intensification. Li *et al.* (2023) revisit the low-latitude problem and highlight that low latitudes enhance the convergent inflow in the boundary layer and depth of convection in the eyewall by reducing the inertial stability in the boundary layer instead of the outflow layer. Beyond the intensification phase, Li and Toumi (2024) found that TCs at lower latitudes decay more quickly after reaching their lifetime maximum intensity, which has not been fully understood.

In summary, while sufficient f may not be necessary for TC formation, it remains an important factor influencing TC development through boundary-layer dynamics. However, it is not clear how a reduced f would affect the development of a pre-existing TC and what the mechanism would be. In particular, this study aims to investigate whether a TC vortex can exist near the Equator under the hypothetical circumstances of no f, focusing on the response of pre-existing TC intensity to the removal of the Coriolis effect.

2 | METHOD

2.1 | Model setup and experimental design

The Weather Research and Forecasting (WRF) model version 4.2.2 (Skamarock *et al.*, 2019) is used to simulate TCs on an idealized aquaplanet with a full-physics parameterization setup. Two nested square domains are used. The side of the outer domain is 5400 km (450 × 450 grid cells, 12-km grid spacing). The inner domain has a side length of 1800 km (450 × 450 grid cells, 4-km grid spacing). The model consists of 41 layers in the vertical from $\sigma = 0$ to $\sigma = 1$, with eight levels under 2 km and 18 levels under 5 km. A full suite of physics schemes is used, including the WRF single-moment six-class microphysics (WSM6) scheme (Hong & Lim, 2006), the Rapid Radiative Transfer Model for general circulation models (RRTMG) scheme (Iacono *et al.*, 2008) for shortwave and longwave radiation, the Yonsei University (YSU) scheme (Hong *et al.*, 2006) for planetary boundary-layer processes, the revised MM5 scheme for surface-layer physics (Fairall *et al.*, 2003; Jiménez *et al.*, 2012), and the New Tiedtke scheme (Zhang & Wang, 2017) for cumulus parameterization in the outer domain.

The sea-surface temperature (SST) is fixed at 27 °C. The initial environmental conditions are specified with moist tropical soundings from Dunion (2011). We initialized the simulations with an axisymmetric vortex with a tangential velocity ($v(r,z,0)$) following Rotunno and Emanuel (1987):

$$v(r,z,0) = \frac{z_* - z}{z_*}\left\langle\left\{v_m^2\left(\frac{r}{r_m}\right)^2\left[\left(\frac{2r_m}{r+r_m}\right)^3 - \left(\frac{2r_m}{r_0+r_m}\right)^3\right] + \frac{f^2r^2}{4}\right\}^{1/2} - \frac{fr}{2}\right\rangle,$$

where r_0 is the outer radius of the vortex beyond which $v = 0$, v_m the maximum wind, and r_m the radius of maximum wind. The intensity decays linearly with height, so that $v = 0$ at $z = z_*$. We also let $v = 0$ for $z > z_*$ and set z_* as 20 km. We choose $r_0 = 412.5$ km, $r_m = 82.5$ km, and $v_m = 15$ m/s. All the simulations are performed in an idealized environment with no environmental flow or shear imposed.

To investigate the impact of a reduced Coriolis parameter f on a developed TC vortex, a series of reduced-f experiments were designed. The control run is conducted on an f-plane at 20°N and lasts for 10 days (*f20*). Sensitivity experiments involved shifting the f-plane from 20° to the Equator (0°) at different rates, both abrupt and gradual,

TABLE 1 List of simulations. The increments are compared with the control one.

Simulations	Changes in f	Restart time	Run time
f20 (Control)	$f = 20°$		240 h
f0	$f = 0°$		216 h
f20-0@72h	$\Delta f = -20°$	$T = 72$ h	120 h
f20-0@96h	$\Delta f = -20°$	$T = 96$ h	120 h
f20-0@120h	$\Delta f = -20°$	$T = 120$ h	120 h
f20-0@144h	$\Delta f = -20°$	$T = 144$ h	120 h
f20-0@168h	$\Delta f = -20°$	$T = 168$ h	120 h
f-varying@144h	$\Delta f = -0.625°$ every 3 h	$T = 144$ h	144 h

Note: The bold font entries (f20, f20-0@144h, and f-varying@144h) are the main experiments analyzed in this work, while the non-bold entries are provided for completeness.

restarting at simulation time 144 h (T_{144}). These were identified as *f20-0@144h* and *f-varying@144h*, respectively. In the *f20-0@144h* experiment, f was instantaneously decreased to zero at T_{144}. Unlike the instantaneous f-plane reductions, the *f-varying@144h* experiment decreased f gradually by 0.625° every 3 h from T_{144}, reaching zero by T_{240}. Note that we use T to denote the absolute simulation time and t to represent the relative time since the restart.

Additional experiments with the same instantaneous change to $f = 0$ were performed at T_{72}, T_{96}, T_{120}, and T_{168} to test the sensitivity to initial TC intensity when f was decreased to zero. An experiment with a constant $f = 0$ throughout (*f0*) was also conducted for comparison. All experiments and the corresponding changes in f are summarized in Table 1. We focus on *f20*, *f20-0@144h*, and *f-varying@144h* to investigate the physical mechanisms underlying the TC intensity response to reduced f (highlighted in Table 1). Results from another group (*f20* and *f20-0@96h*) showing consistent responses are included in the Supporting Information (see Figure S1–S7).

2.2 | Gradient wind balance

Except in the surface frictional boundary layer and the outflow layer, where friction and radial acceleration are not negligible, gradient wind balance is essential to controlling the primary circulation in intense storms. The gradient balance describes the balance between three key forces that govern the motion of air parcels around the cyclone: the centrifugal force, the pressure gradient force, and the Coriolis force. The impact of zero f on the gradient wind balance and TC circulation will be one focus of this study. The gradient wind equation can be expressed as

$$\frac{V_{\mathrm{gr}}^2}{r} + fV_{\mathrm{gr}} = \frac{1}{\rho}\frac{\partial p}{\partial r},$$

where V_{gr} is the gradient wind (which approximates the tangential wind), r is the radial distance from the TC centre, f is the Coriolis parameter, ρ is the air density, and $\partial p/\partial r$ is the radial pressure gradient.

3 | RESULTS

3.1 | Simulations

Figure 1a illustrates the intensity evolution of simulated TCs listed in Table 1. In the control experiment (*f20*), the TC remains in a stable mature phase following its developmental stage, while in the case of a constant $f = 0$ (*f0*) the hurricane strength threshold cannot be held after the initial spin-up. In the reduced-f experiments, TC intensity decreases after a temporary intensification as f is decreased. While the weakest storm (*f20-0@72h*) and the storm under varying f (*f-varying@144h*) can maintain at Saffir–Simpson CAT 1 (Simpson & Saffir, 1974) with decreasing f, the other simulated TCs dissipate completely. Stronger storms decay faster compared with weaker storms. The weakening rates of the first 24 hours are 12.1, 12.7, 17.4, 20.7, and 30.5 m/s for *f20-0@72h*, *96h*, *120h*, *144h*, and *168h*, respectively.

The set of comparable experiments restarted at T_{144} is shown in Figure 1b. In *f20-0@144h*, a rapid weakening occurs after a temporary intensification, followed by another rapid weakening starting at t_{60}. In *f-varying@144h*, TC intensity decreases followed by a 26-hour stable period. The weakening mechanisms under zero f are examined at t_6 for *f20-0@144h* and at t_{48} for *f-varying@144h*.

Comparisons of axisymmetric TC wind structure between *f20* and reduced-f experiments are shown in Figures 2 and 3. At t_6, the reduced-f experiments showed a temporary strengthening of both inflow and outflow throughout the entire cyclone depth (Figure 2b,d,f).

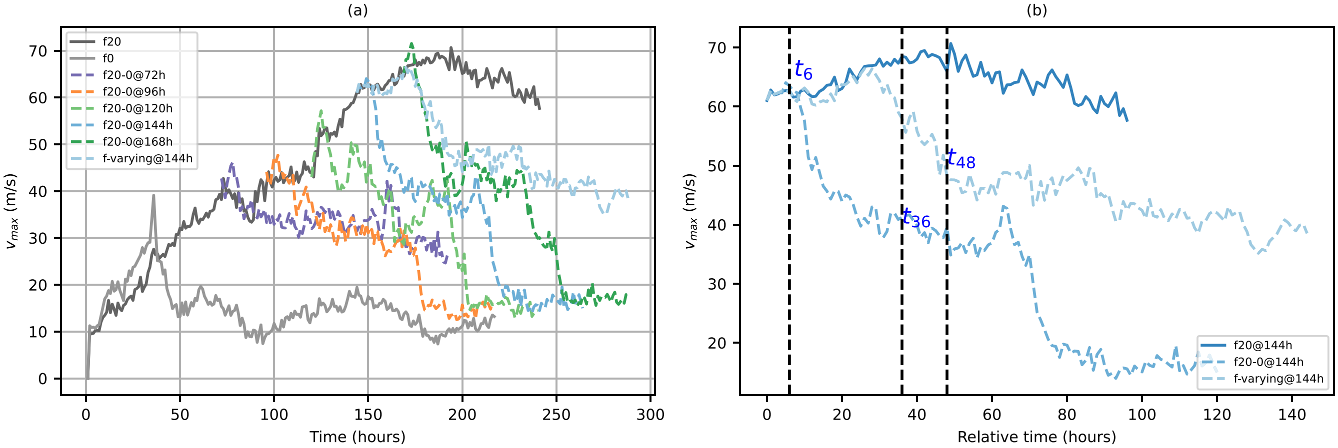

FIGURE 1 (a) Time evolution of the maximum surface wind ($v_{\max}$) from the control experiment and seven reduced-f experiments. (b) Time evolution of $v_{\max}$ from three comparable experiments: *f20*, *f20-0@144h*, and *f-varying@144h*, relative to the restart time at T_{144}. The vertical dashed lines (t_6, t_{36}, and t_{48}) mark the key points for subsequent analysis.

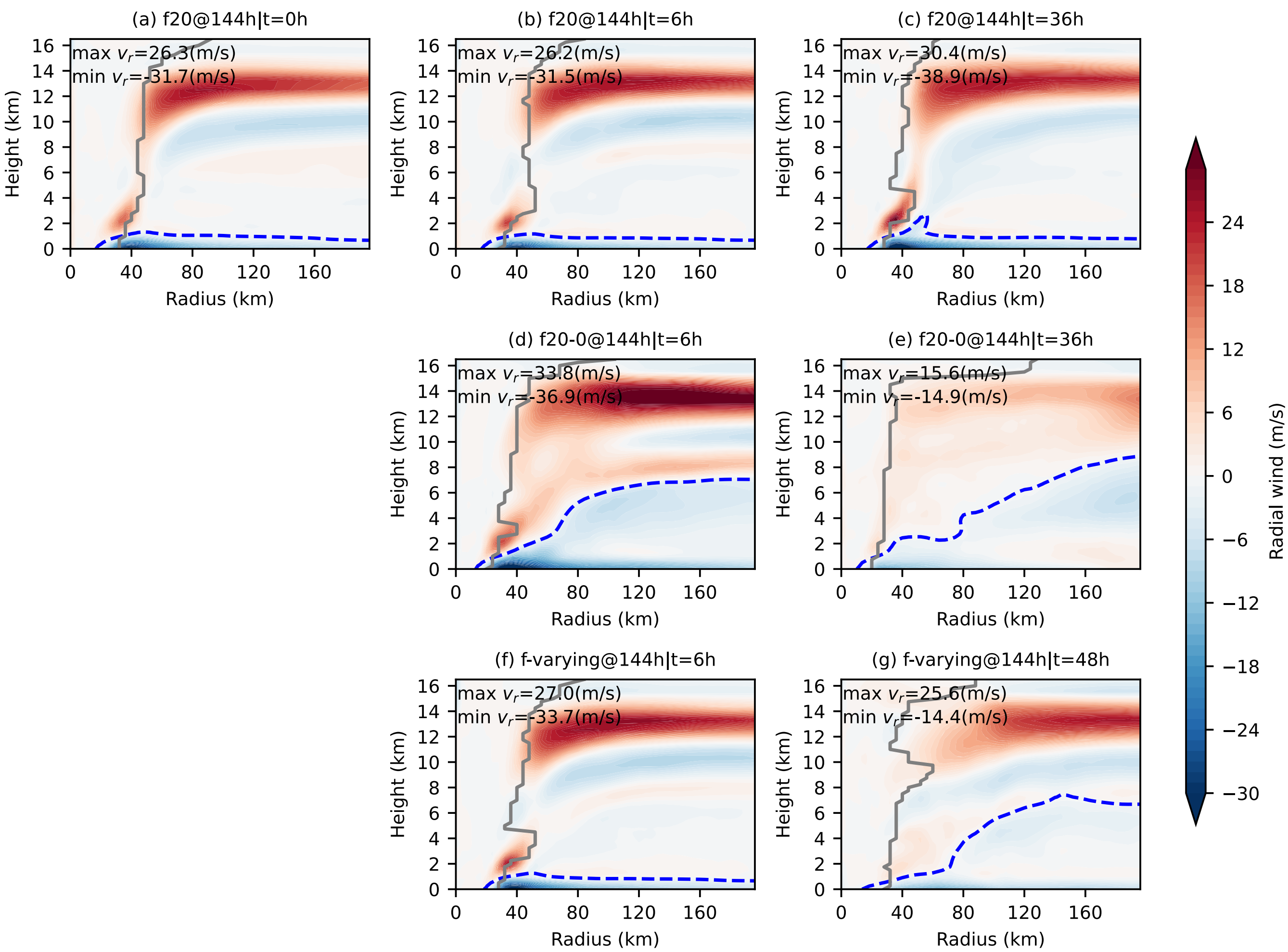

FIGURE 2 Height–radius plots of the azimuthally averaged tangential wind (contours) and radial wind (shading) from experiments *f20* (first row), *f20-0@144h* (second row), and *f-varying@144h* (third row) at $t = 0$ h (first column), 6 h (second column), and 36/48 h (third column). The annotations in the top left corner of each panel give the maximum and minimum radial wind. The blue contours, defined as 5% of the maximum radial inflow, represent the inflow layer height. The grey dashed lines indicate the radius of maximum wind at each level for each snapshot.

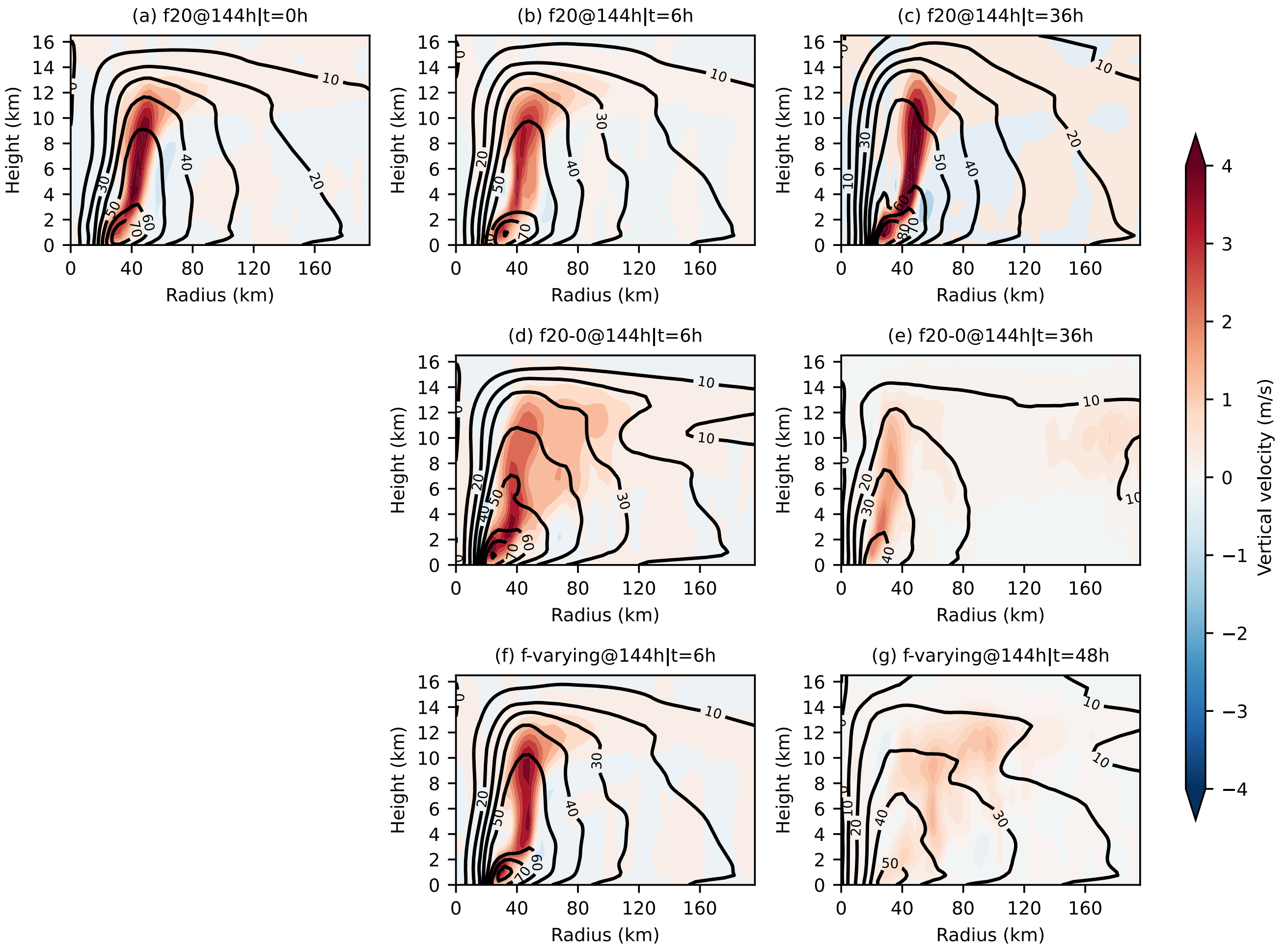

FIGURE 3 Height–radius plots of the azimuthally averaged vertical velocity (shading) and tangential wind (contours) from experiments *f20* (first row), *f20-0@144h* (second row), and *f-varying@144h* (third row) at $t = 0$ h (first column), 6 h (second column), and 36/48 h (third column).

The strengthening of inflow at the low and mid-levels is associated with an increase in inflow layer height (Figure 2d), which is defined by 5% of the maximum radial inflow (Zhang *et al.*, 2011). During the weakening stage, *f20-0@144h* showed significant decline of both inflow and outflow at t_{36} (Figure 2e); *f-varying@144h* showed limited change in the strength of upper-level outflow but an outward shift at t_{48} (Figure 2g). The reduced-f experiments both showed a large inflow layer height.

Regarding vertical motion, *f20-0@144h* showed that the sloping updrafts extended outward above 5 km at t_6 (Figure 3d) and declined by t_{36} (Figure 3e). In *f-varying@144h*, the sloping updrafts broadened outward above 5 km and were reduced significantly at t_{48} (Figure 3g). The expansion of updrafts above 5 km relates to the expansion of deep convection (Figure 4b,c). Deep convection is evidenced by radar reflectivity greater than 20 dBZ at 10 km altitude (Rogers *et al.*, 2020; Stone *et al.*, 2023; Wadler *et al.*, 2023); Figure 4). The expansion of deep convection is attributed to strengthened low-level inflow, which enhances convergence outside the eyewall (Figure 2). While the low-level updrafts outside the eyewall can be offset by downdrafts from evaporative cooling, the expansion of updrafts persists above 5 km.

Alongside the more active deep convection in the outer rainbands (Figure 4b,c) there are more pronounced convective updrafts and downdrafts (Figure 5b,c). The downdrafts occur on the convective scale and typically form due to evaporative cooling of precipitation in mid-levels outside the eyewall and in outer rainbands. The convective downdrafts play an important vertical mixing role in bringing low θ_e mid-tropospheric air to the surface (Chan & Kepert, 2010).

3.2 | Reduction in equivalent potential temperature in the boundary layer

To investigate the decay under zero f, we examine the changes in equivalent potential temperature (θ_e) below

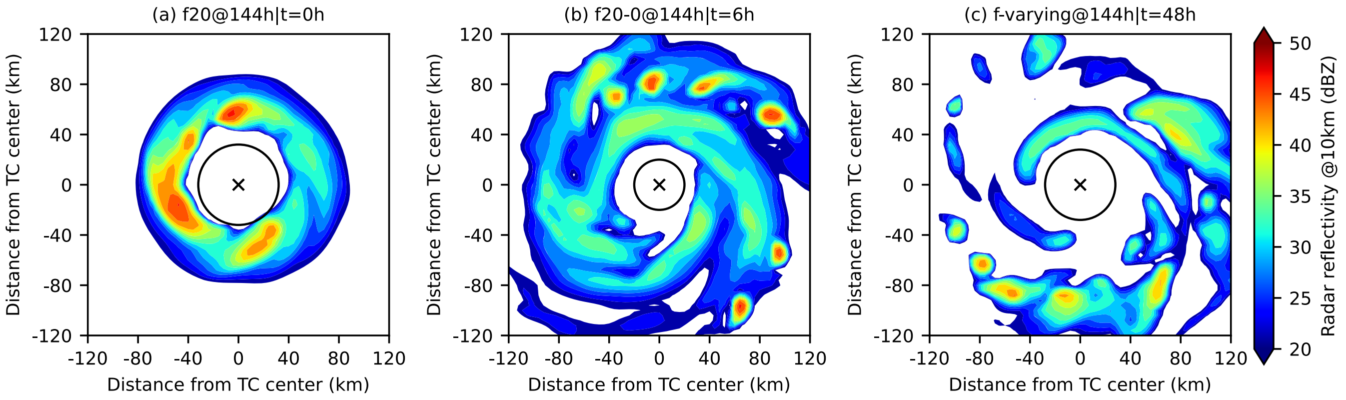

FIGURE 4 Horizontal cross-sections of radar reflectivity greater than 20 dBZ at a height of 10 km around the TC centre for (a) the initial state, (b) *f20-0@144h* at $t = 6$ h, and (c) *f-varying@144h* at $t = 48$ h. The circles indicate the radius of maximum wind for each snapshot.

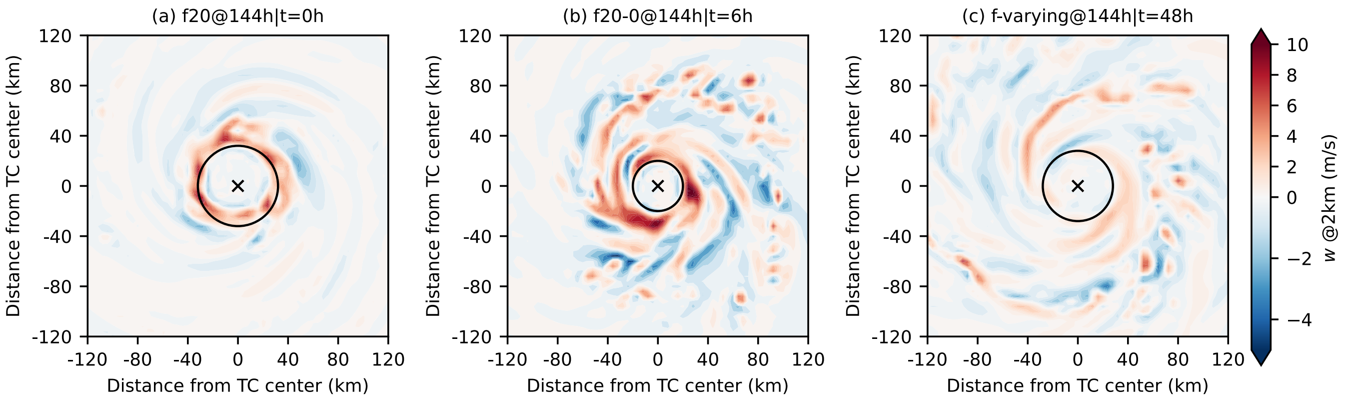

FIGURE 5 Horizontal cross-sections of vertical velocity (w) at a height of 2 km around the TC centre for (a) the initial state, (b) *f20-0@144h* at $t = 6$ h, and (c) *f-varying@144h* at $t = 48$ h. The circles indicate the radius of maximum wind for each snapshot.

1.5 km, which is the typical height of the boundary layer in TCs (approximately 0.5–1.5 km: Kepert, 2001). Figure 6 shows the time evolution of θ_e within the boundary layer (BL). A pronounced decrease in θ_e, approximately 12 K near the eyewall region, is observed from t_6 in *f20-0@144h*. In the *f-varying@144h* scenario, a minor decrease in θ_e occurred until a noticeable decline was observed starting at t_{48}. If the θ_e reduction in the BL cannot be recovered by the surface flux, the low-θ_e air feeding into the eyewall will suppress the eyewall convection and cause a weakening of the TC (Alland *et al.*, 2021a; Riemer *et al.*, 2010).

Why does the θ_e in the BL decrease for smaller f? The deepening of the inflow layer (e.g., Figure 2d) and increasing downdrafts (e.g., Figure 5b) come into our consideration.

The inflow layer height in the reduced-f experiments has increased significantly due to the enhancement of radial inflow at the low and mid-levels (e.g., Figure 2d). Meanwhile, the distribution of θ_e shows high values in the BL and low values in the mid-levels (approximately 3–8 km altitude: Figure 7b,c), confirming that the free troposphere is the source of low θ_e (Simpson & Riehl, 1958). Therefore, a deeper inflow layer would enhance the entrainment of dry air from the mid-levels, leading to a reduction in θ_e within the BL.

Moreover, the reduced-f experiments have stronger downdrafts in the outer rainbands (Figures 5 and 7). The strengthened downdrafts would also carry low-θ_e air from the mid-troposphere to the BL. Collectively, the combined effects of the highly elevated inflow layer and the enhanced downdrafts outside the eyewall will enhance the entrainment of low-θ_e air into the inflow layer and lower the θ_e in the BL, thereby disrupting the energy production necessary for sustaining deep convection.

3.3 | Gradient imbalance analysis

Agradient force (AGF) is a key force in driving the radial wind. It arises when the gradient wind balance is

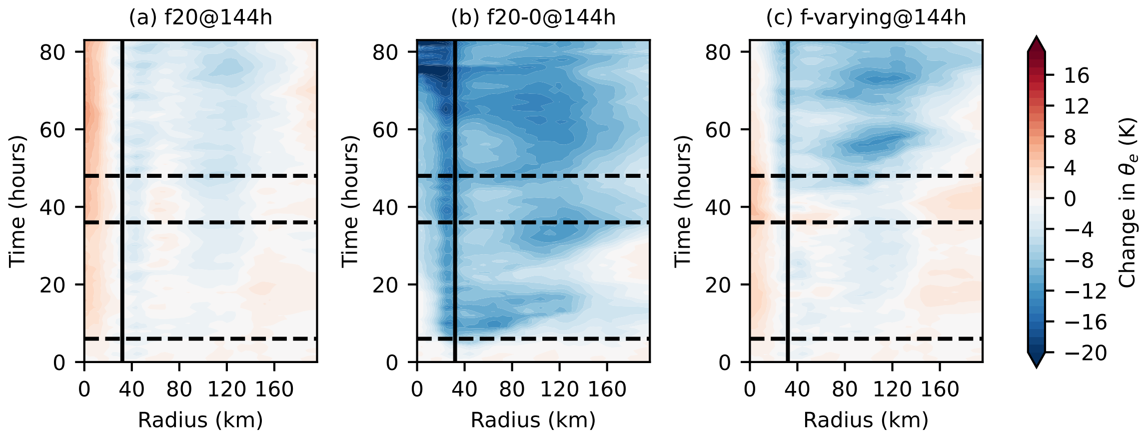

FIGURE 6 Time–radius plots of changes in azimuthally averaged equivalent potential temperature (θ_e) under 1.5 km relative to its initial restart value. Black dashed lines indicate $t = 6$, 36, and 48 h after reduction f. Vertical lines mark the radius of maximum wind at t_0 for each case.

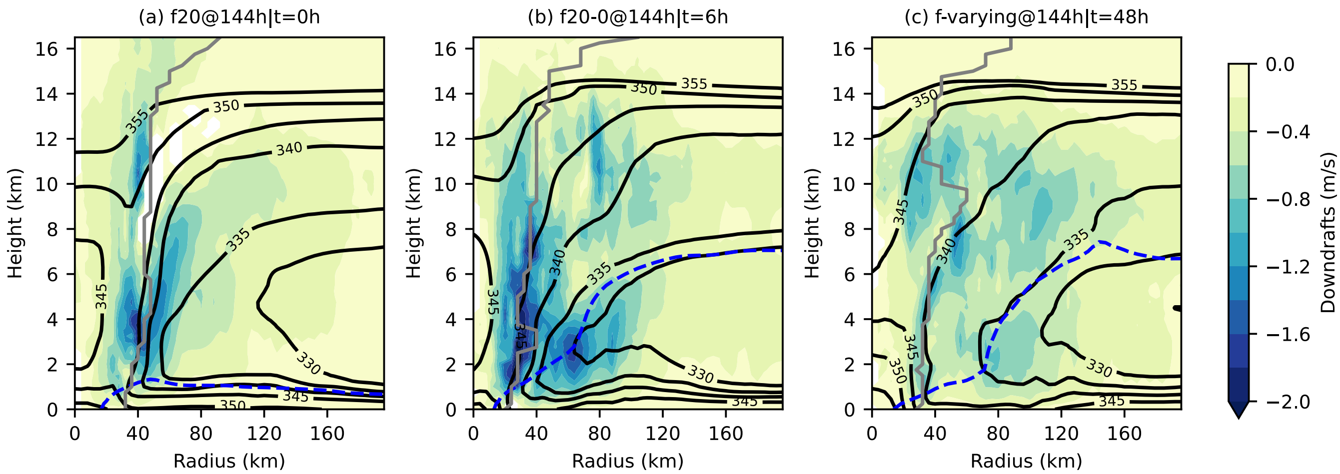

FIGURE 7 Height–radius plot of the azimuthally averaged negative vertical velocity (shading) and θ_e (contours) for (a) the initial state, (b) *f20-0@144h* at $t = 6$ h, and (c) *f-varying@144h* at $t = 48$ h. The blue dashed contours represent 5% of the maximum radial inflow. The grey dashed lines indicate the radius of maximum wind for each snapshot.

unbalanced, which can be given as

$$AGF = \frac{V_{\mathrm{gr}}^2}{r} + fV_{\mathrm{gr}} - \frac{1}{\rho}\frac{\partial p}{\partial r}.$$

An outward agradient force (supergradient force) accelerates radial outflow, while an inward agradient force (subgradient force) accelerates radial inflow. The comparison of the agradient force for the three experiments outside the eyewall region (> 40 km) is shown in Figure 8a–c. Figure 8d–f shows the pressure gradient force, while Figure 8g–i shows the combined centrifugal and Coriolis forces, illustrating the components of the gradient imbalance.

In the outer-core region (40–160 km) and lower to mid-troposphere (0–10 km), the reduced-f experiments show an enhanced subgradient force (Figure 8b,c), which can accelerate the radial inflow. They also show a decrease in centrifugal and Coriolis forces (Figure 8h,i), consistent with the enhanced subgradient force, while the low-level pressure gradient force remains largely unchanged (Figure 8e,f). This indicates that the reduced centrifugal and Coriolis forces under the smaller f are responsible for the enhanced subgradient force at low to mid-levels at t_6.

In the mid to upper troposphere (above 6 km) near the eyewall (40–80 km radius), the reduced-f experiments show a much stronger supergradient force than the control run (e.g., Figure 8d), contributing to a stronger upper-level outflow. Figure 8e shows an increased outward pressure gradient force, aligning with the enhanced supergradient force. In contrast, changes in centrifugal and Coriolis

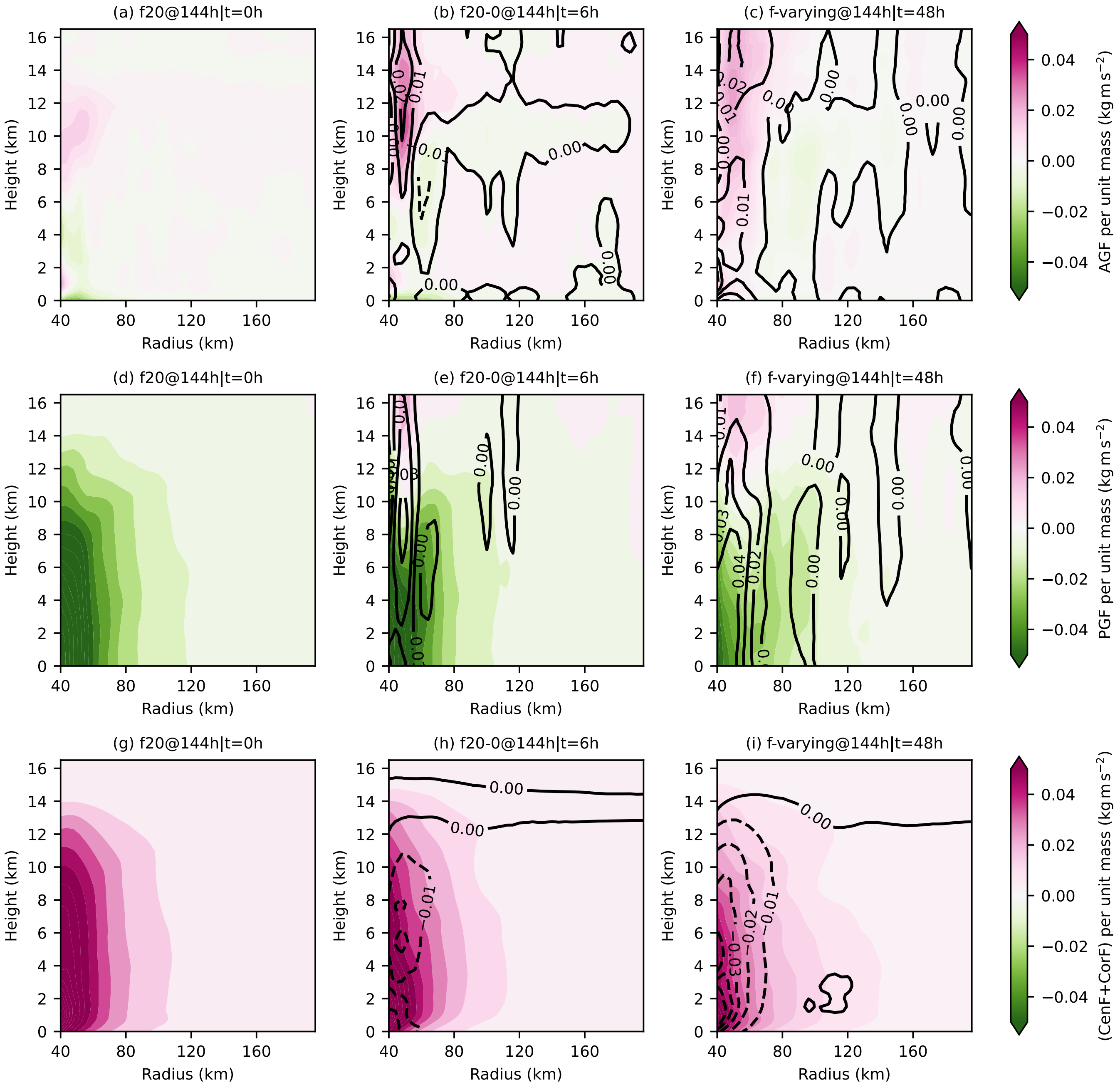

FIGURE 8 Height–radius plots of the azimuthally averaged forces: agradient force (AGF, shading, first row), pressure gradient force (PGF, shading, second row), and the sum of centrifugal and Coriolis forces (CenF+CorF, shading, third row), shown for the initial state (first column), *f20-0@144h* at $t = 6$ h (second column), and *f-varying@144h* at $t = 48$ h (third column). Contours indicate changes from the initial state with a 0.01 interval in $\mathrm{kg \cdot m \cdot s^{-2}}$.

forces oppose the agradient change (Figure 8h). These results suggest that the increased pressure gradient force is responsible for the stronger upper-level supergradient flow.

Inertial stability describes how resistant the TC circulation is to changes or perturbations in the radial direction. High inertial stability means that the system strongly resists such changes, maintaining a stable and tightly wound circulation. Inertial stability can be expressed as follows:

$$I^2 = \left(\frac{\partial r v_t}{r \partial r} + f_0\right)\left(f_0 + \frac{2v_t}{r}\right),$$

where I^2 is inertial stability, r is the radial distance from the TC center, v_t is the tangential wind, and f_0 is the Coriolis parameter at the TC center.

Figure 9 illustrates the distribution of I^2. Due to a substantial decrease of f in *f20-0@144h*, there is a significant decrease in I^2 near the eyewall caused by the shrinkage

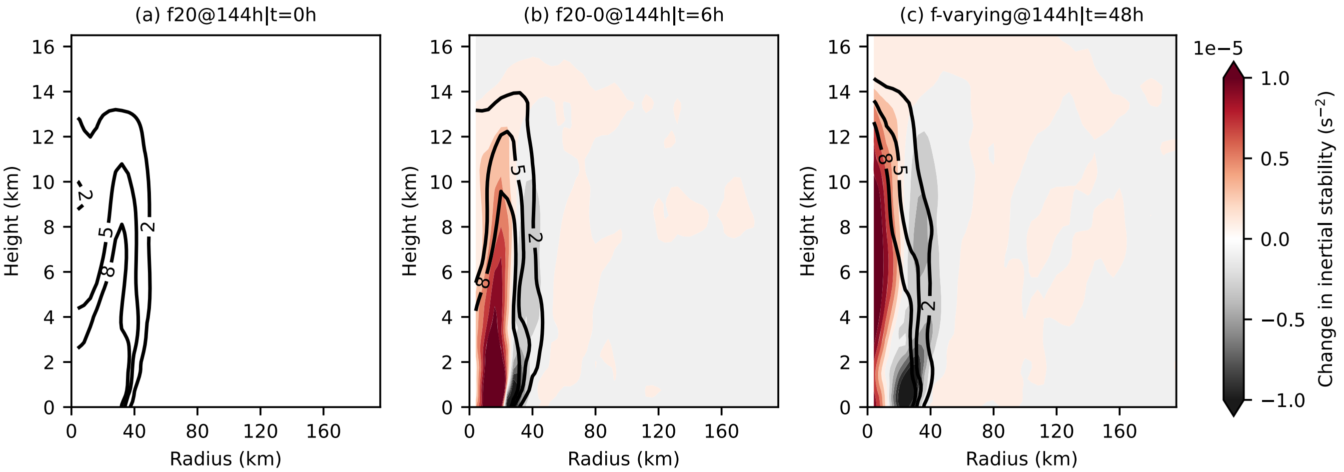

FIGURE 9 Height–radius plots of the azimuthally averaged inertial stability (I^2, contours) and changes in I^2 (shading) relative to restart time for (a) the initial state, (b) *f20-0@144h* at $t = 6$ h, and (c) *f-varying@144h* at $t = 48$ h. The contours have an interval of 3×10^{-6} s^{-2}.

of maximum wind speed during intensification at t_6, with relatively smaller changes observed in the outer-core region (Figure 9b). While the quantity of I^2 is directly related to both the storm's intensity and the change in f, the net effect from f was evaluated by computing the changes in the I^2 field before and after the reduction of f_0 to zero at t_6. We find a median decrease of approximately 1.26×10^{-8} s^{-2} in I^2, compared with the actual decrease of 1.46×10^{-8} s^{-2} in I^2 outside the radius of 80 km. This confirms the relatively significant role of f in the outer-core region. Collectively, the decline in I^2 in the outer-core region, along with enhanced agradient forcing (Figure 8b,c), can thus drive stronger radial inflow at low to mid-levels and stronger radial outflow aloft.

The changes in radial wind driven by agradient force can change the TC intensity by transporting absolute angular momentum. The absolute angular momentum (AAM) per unit mass of an air parcel about the rotation axis is denoted as

$$AAM = rv_{\mathrm{t}} + \frac{1}{2} f r^2,$$

where v_{t} is the tangential wind, rv_{t} is the relative angular momentum, and $\frac{1}{2} f r^2$ is the planetary angular momentum. The radial transport of AAM (AAMF) towards the TC centre at each point is given by

$$AAMF = v_r \cdot AAM.$$

Radial inflow contributes to vortex spin-up by transporting angular momentum inward, partially offsetting losses due to frictional dissipation near the surface. Figure 10 shows the radial transport of AAM in the three experiments. AAM generally increases with radius due to its radial dependence, but under reduced f it decreases notably in the outer region (Figure 10b,c). Despite radial inflow strengthening at low and mid-levels, it may bring less AAM into the inner core if the overall AAM reservoir is reduced. Previous research has also shown that the changes in TC intensity are positively related to the changes in upper-level AAM export (Chan & Chan, 2013).

3.4 | Summary

Figure 11 presents a schematic illustrating the potential mechanisms by which a developed TC responds to a reduced Coriolis parameter (f). Based on our analysis, the direct effect of zero-f on TCs is the reduction of inertial stability and increased agradient force in the outer-core region, which can strengthen further both the radial inflow and outflow throughout the storm's depth. The enhanced radial inflow will not only deepen the inflow layer but also facilitate convergence, thereby intensifying deep convection and strengthening downdrafts in the outer rainbands. However, the deepened inflow layer combined with enhanced downdrafts could promote greater entrainment of dry air from the free troposphere, which in turn would lower the boundary layer θ_{e} and cause decay. This TC weakening can be explained by the following processes: the lowering BL θ_{e} reduces the vertical gradient of θ_{e}, thereby stabilizing the atmosphere and suppressing deep convection along with the associated diabatic heating. This weakens upward motion and the radial gradient of pressure, consequently causing a diminished secondary circulation. When radial inflow can no longer offset frictional loss by importing angular momentum, the TC decays. The decrease in AAM export through upper-level outflow can aid further in this weakening process.

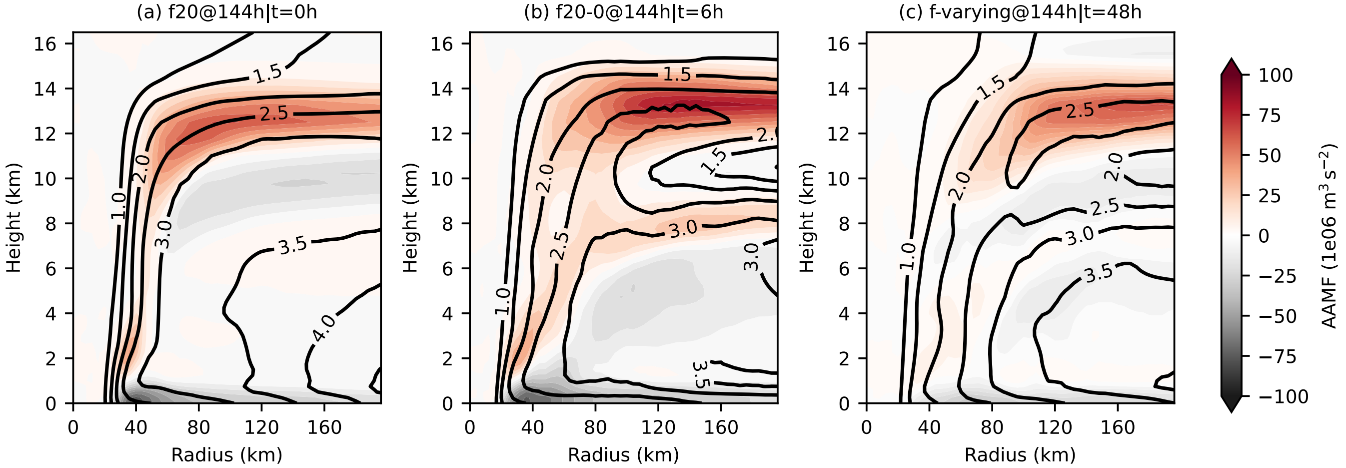

FIGURE 10 Height–radius plots of the azimuthally averaged radial flux of absolute angular momentum (AAMF, shading) for (a) the initial state, (b) *f20-0@144h* at $t = 6$ h, and (c) *f-varying@144h* at $t = 48$ h. The contours show the value of absolute angular momentum with an interval of 5×10^5 m$^2 \cdot$ s^{-1}.

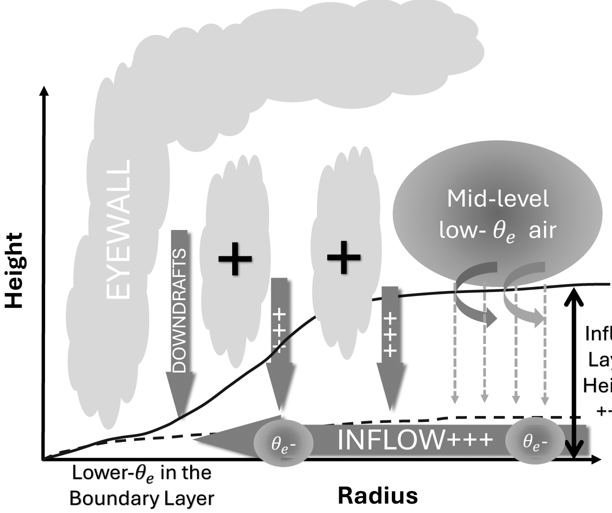

FIGURE 11 Schematic diagram indicating the decay mechanism under reduced f: the deepening of the inflow layer height accompanied by strengthened downdrafts enhances the entrainment of low-θ_e air from mid-levels, which leads to the reduction of θ_e in the boundary layer.

4 | DISCUSSION

A sufficient Coriolis effect is one of the key factors influencing the formation and development of TCs. However, it is not clear how a lower latitude would affect an already developed TC vortex. This study investigates the response of TC intensity to the reduction of f and reveals that TCs gradually weaken as f is removed. The key effect of reduced f on this decay process lies in the deepening of the inflow layer and the enhancement of downdrafts in the outer rainbands, which is associated with the strengthening of radial inflow in the absence of f. The deeper inflow layer depth and enhanced downdrafts introduce low-θ_e air into the BL, leading to the weakening of convection and TCs to decay. However, it is acknowledged that both the inflow and outflow are amplified due to the reduction of f, with in/outflow patterns strengthening throughout the cyclone depth.

The impact of low latitude (f) on a developed TC vortex differs from that on TC formation and intensification. During TC formation, sufficient f facilitates spin-up by rotating convergent flow and creating angular momentum (Briegel & Frank, 1997; Gray, 1968, 1979, 1985, 1998). For TC intensification, the stronger BL inflow associated with lower latitudes will bring more angular momentum into the system, promoting faster intensification (Li *et al.*, 2012, 2023; Smith *et al.*, 2015). However, in the case of an already developed TC vortex, the enhancement of the low-level inflow combined with enhanced downdrafts disrupts the BL by entraining more low-θ_e air from mid-levels. Li and Toumi (2024) show that TCs decay more quickly with a smaller initial f. Although the phenomenon might not be fully linked to the decreasing f scenario in this study, stronger radial inflow at lower latitudes likely leads to faster decay.

The weakening rate of the first 24-hour decay is proportional to TC intensity, with the strongest storm showing the largest weakening rate (Figure 1a). Sensitivity experiments with zero-f initiated earlier at T_{96} are presented in the Supporting Information (Figures S1–S7). The same mechanism is discernible in this analysis, characterized by enhanced radial inflow and outflow, the presence of downdrafts external to the eyewall, and a marked reduction in θ_e within the boundary layer. However, it has a lower weakening rate of 12.7 m/s compared with 20.7 m/s at T_{144}. This is consistent with existing observations, which suggest that stronger storms usually decay faster than weaker storms (Wang *et al.*, 2020). Notably, the stronger storm shows more intense downdrafts near the eyewall (comparing Figures 7b and S7b), resulting in a more substantial decrease in θ_e in that region (comparing Figures 6b and S6b). This result suggests that the influence of zero-f on weakening rate may depend on the strength of downdrafts, which is expected to increase with TC intensity.

The deeper inflow layer height under lower f in this study also aligns with theoretical studies. The inflow layer height is commonly used as a dynamical definition for the boundary-layer height in TCs (Zhang *et al.*, 2011, 2023). Theoretical studies indicate that the boundary-layer height is inversely proportional to the square root of inertial stability (I) at the top of the boundary layer, expressed as $D_e = (2K/I)^{1/2}$, where K is the turbulent diffusivity (Kepert & Wang, 2001). As I is typically proportional to the Coriolis parameter f, this relationship implies that boundary-layer height increases when f (and thus I) decreases. This is consistent with the increased inflow layer height observed under reduced f conditions in our results. Outside the core region, where inertial stability is lower and the Coriolis parameter f plays a relatively greater role, the boundary-layer height is more sensitive to reductions in f. This is consistent with our findings that the inflow layer deepens more significantly in the outer-core region under reduced f conditions.

The mechanisms identified in this study share notable similarities with those previously proposed for TC weakening under vertical wind shear (Alland *et al.*, 2021a, 2021b; Riemer *et al.*, 2010). Shear-induced downward transport of low-equivalent potential temperature (θ_e) air into the boundary layer has been shown to reduce TC intensity from the view of a Carnot-cycle heat engine for intense TCs in shear (Riemer *et al.*, 2010). In particular, radial and downdraft ventilation associated with vortex tilt under shear were shown to contribute to this weakening by transporting low-θ_e air inward and downward, respectively, which suppresses inner-core upward mass flux and limits the spatial extent of strong convection (Alland *et al.*, 2021a, 2021b). Interestingly, the dynamic response observed in the reduced-f experiments exhibits effects comparable with shear. However, unlike shear-induced cases, no vertical wind shear is imposed in this study, and no significant vortex tilt develops, with maximum changes of 4.2 and 2.4 km in *f20-0@144h* (mean tilt = 6.3 km) and *f-varying@144h* (mean tilt = 6.5 km), respectively, compared with the control (mean tilt = 5.4 km) during the first 24 hours after restart, thereby validating the thermodynamic decay method irrespective of shear or zero f. Other dynamical processes, such as outflow layer dynamics, increased frictional dissipation, and potential eyewall replacement cycles, may also influence TC weakening; however, these are not explored and are outside the scope of this study. Regardless of that, we find that the combined effect of increasing inflow layer depth and downdrafts is the main cause of decay under the pure modification of f.

5 | CONCLUSIONS

This study aimed to investigate the response of a pre-existing TC vortex to the removal of the Coriolis effect. It is found that TCs decay gradually under extremely reduced f. The deepening of the inflow layer and reduction in θ_e in the boundary layer were considered as the key to causing TC weakening. These findings provide a deeper understanding of how the Coriolis effect can affect intensity evolution, in particular the declining phase of the TC life cycle. This study implies that, while TCs may not form near the Equator, a TC steered equatorward could persist for several days despite gradual weakening, posing a potential threat to vulnerable and unprepared communities in equatorial regions.

ACKNOWLEDGEMENTS

This work was supported by the Natural Environmental Research Council (NE/W009587/1), the Singapore Green Finance Centre, and the Vodafone foundation (DreamLab project). DreamLab users provided their phone computing power and time.

CONFLICT OF INTEREST STATEMENT

The authors declare that they do not have any conflict of interest.

DATA AVAILABILITY STATEMENT

The data that support the findings of this study are available from the corresponding author upon reasonable request.

ORCID

Min Li https://orcid.org/0000-0002-8212-7843

REFERENCES

Alland, J.J., Tang, B.H., Corbosiero, K.L. & Bryan, G.H. (2021a) Combined effects of midlevel dry air and vertical wind shear on tropical cyclone development. Part I: downdraft ventilation. *Journal of the Atmospheric Sciences*, 78(3), 763–782.

Alland, J.J., Tang, B.H., Corbosiero, K.L. & Bryan, G.H. (2021b) Combined effects of midlevel dry air and vertical wind shear on tropical cyclone development. Part II: radial ventilation. *Journal of the Atmospheric Sciences*, 78(3), 783–796.

Briegel, L.M. & Frank, W.M. (1997) Large-scale influences on tropical cyclogenesis in the western north pacific. *Monthly Weather Review*, 125(7), 1397–1413.

Chan, J.C.L. & Kepert, J.D. (2010) *Global perspectives on tropical cyclones: from science to mitigation*. books.google.com

Chan, K.T.F. & Chan, J.C.L. (2013) Angular momentum transports and synoptic flow patterns associated with tropical cyclone size change. *Monthly Weather Review*, 141(11), 3985–4007.

Chang, C.-P., Liu, C.-H. & Kuo, H.-C. (2003) Typhoon vamei: an equatorial tropical cyclone formation. *Geophysical Research Letters*, 30(3), 1–4.

DeMaria, M. & Pickle, J.D. (1988) A simplified system of equations for simulation of tropical cyclones. *Journal of the Atmospheric Sciences*, 45(10), 1542–1554.

Dunion, J.P. (2011) Rewriting the climatology of the tropical north Atlantic and Caribbean Sea atmosphere. *Journal of Climate*, 24(3), 893–908.

Fairall, C.W., Bradley, E.F., Hare, J.E., Grachev, A.A. & Edson, J.B. (2003) Bulk parameterization of air–sea fluxes: updates and verification for the COARE algorithm. *Journal of Climate*, 16(4), 571–591.

Gray, W.M. (1968) Global view of the origin of tropical disturbances and storms. *Monthly Weather Review*, 96(10), 669–700.

Gray, W.M. (1979) *Hurricanes: their formation, structure and likely role in the tropical circulation. Meteorology over the tropical oceans*. cir.nii.ac.jp.

Gray, W.M. (1985) Tropical cyclone global climatology. *WMO Technical Document WMO/TD*, 72(1), 3–19.

Gray, W.M. (1998) The formation of tropical cyclones. *Meteorology and Atmospheric Physics*, 67(1–4), 37–69.

Hong, S.-Y. & Lim, J.J.-O. (2006) The WRF single-moment 6-class microphysics scheme (WSM6). *Journal of the Korean Meteorological Society*, 42, 129–151.

Hong, S.-Y., Noh, Y. & Dudhia, J. (2006) A new vertical diffusion package with an explicit treatment of entrainment processes. *Monthly Weather Review*, 134(9), 2318–2341.

Iacono, M.J., Delamere, J.S., Mlawer, E.J., Shephard, M.W., Clough, S.A. & Collins, W.D. (2008) Radiative forcing by long-lived greenhouse gases: calculations with the AER radiative transfer models. *Journal of Geophysical Research: Atmospheres*, 113(D13), 2008JD009944.

Jiménez, P.A., Dudhia, J., González-Rouco, J.F., Navarro, J., Montávez, J.P. & García-Bustamante, E. (2012) A revised scheme for the WRF surface layer formulation. *Monthly Weather Review*, 140(3), 898–918.

Kepert, J. (2001) The dynamics of boundary layer jets within the tropical cyclone core. Part I: linear theory. *Journal of the Atmospheric Sciences*, 58(17), 2469–2484.

Kepert, J. & Wang, Y. (2001) The dynamics of boundary layer jets within the tropical cyclone core. Part II: nonlinear enhancement. *Journal of the Atmospheric Sciences*, 58, 2485–2501.

Kilroy, G., Smith, R.K. & Montgomery, M.T. (2020) An idealized numerical study of tropical cyclogenesis and evolution at the equator. *Quarterly Journal of the Royal Meteorological Society*, 146(727), 685–699.

Li, M. & Toumi, R. (2024) On the temporal decay of tropical cyclones over the ocean. *Geophysical Research Letters*, 51(23), 1–9.

Li, T., Ge, X., Peng, M. & Wang, W. (2012) Dependence of tropical cyclone intensification on the Coriolis parameter. *Tropical Cyclone Research and Review*, 1(2), 242–253.

Li, Y., Wang, Y. & Tan, Z.-M. (2023) Is the outflow-layer inertial stability crucial to the energy cycle and development of tropical cyclones? *Journal of the Atmospheric Sciences*, 80(6), 1605–1620.

Merrill, R.T. (1984) A comparison of large and small tropical cyclones. *Monthly Weather Review*, 112(7), 1408–1418.

Rappin, E.D., Morgan, M.C. & Tripoli, G.J. (2011) The impact of outflow environment on tropical cyclone intensification and structure. *Journal of the Atmospheric Sciences*, 68(2), 177–194.

Riemer, M., Montgomery, M.T. & Nicholls, M.E. (2010) A new paradigm for intensity modification of tropical cyclones: thermodynamic impact of vertical wind shear on the inflow layer. *Atmospheric Chemistry and Physics*, 10(7), 3163–3188.

Rogers, R.F., Reasor, P.D., Zawislak, J.A. & Nguyen, L.T. (2020) Precipitation processes and vortex alignment during the intensification of a weak tropical cyclone in moderate vertical shear. *Monthly Weather Review*, 148(5), 1899–1929.

Rotunno, R. & Emanuel, K.A. (1987) An Air–Sea interaction theory for tropical cyclones. Part II: evolutionary study using a nonhydrostatic axisymmetric numerical model. *Journal of the Atmospheric Sciences*, 44(3), 542–561.

Simpson, R. & Riehl, H. (1958) Mid-tropospheric ventilation as a constraint on hurricane development and maintenance. In: *Preprints, Technical Conference on Hurricanes*. Miami Beach, FL: American Meteorological Society, pp. D4–1–D4–10.

Simpson, R. & Saffir, H. (1974) The hurricane disaster–potential scale. *Weatherwise*, 27(4), 169–186.

Skamarock, W.C., Klemp, J.B., Dudhia, J., Gill, D.O., Liu, Z., Berner, J. et al. (2019) *A description of the advanced research WRF version 4. Technical Note NCAR/TN-556+STR, National Center for Atmospheric Research (NCAR)*.

Smith, R.K., Kilroy, G. & Montgomery, M.T. (2015) Why do model tropical cyclones intensify more rapidly at low latitudes? *Journal of the Atmospheric Sciences*, 72(5), 1783–1804.

Smith, R.K., Schmidt, C.W. & Montgomery, M.T. (2011) An investigation of rotational influences on tropical-cyclone size and intensity. *Quarterly Journal of the Royal Meteorological Society*, 137(660), 1841–1855.

Sparks, N. & Toumi, R. (2024) The ImpeRIal college storm model (IRIS) dataset. *Scientific Data*, 11(1), 424.

Steenkamp, S.C., Kilroy, G. & Smith, R.K. (2019) Tropical cyclogenesis at and near the equator. *Quarterly Journal of the Royal Meteorological Society*, 145(722), 1846–1864.

Stone, Z., Alvey, G.R., Dunion, J.P., Fischer, M.S., Raymond, D.J., Rogers, R.F. et al. (2023) Thermodynamic contribution to vortex alignment and rapid intensification of hurricane sally (2020). *Monthly Weather Review*, 151(4), 931–951.

Wadler, J.B., Cione, J.J., Rogers, R.F. & Fischer, M.S. (2023) On the distribution of convective and stratiform precipitation in tropical cyclones from airborne Doppler radar and its relationship to intensity change and environmental wind shear direction. *Monthly Weather Review*, 151(12), 3209–3233.

Wang, S., Rashid, T. & Throp, H. (2020) A shortening of the life cycle of major tropical cyclones. *Geophysical Research Letters*, 47, 1–8.

Wang, S. & Toumi, R. (2022) An analytic model of the tropical cyclone outer size. *NPJ Climate and Atmospheric Science*, 5(1), 1–10.

Young, R. & Hsiang, S. (2024) Mortality caused by tropical cyclones in the United States. *Nature*, 635(8037), 121–128.

Zhang, C. & Wang, Y. (2017) Projected future changes of tropical cyclone activity over the western north and south pacific in a 20-km-mesh regional climate model. *Journal of Climate*, 30(15), 5923–5941.

Zhang, J.A., Rogers, R.F., Nolan, D.S. & Marks, F.D. (2011) On the characteristic height scales of the hurricane boundary layer. *Monthly Weather Review*, 139(8), 2523–2535.

Zhang, J.A., Rogers, R.F., Reasor, P.D. & Gamache, J. (2023) The mean kinematic structure of the tropical cyclone boundary layer and its relationship to intensity change. *Monthly Weather Review*, 151(1), 63–84.

SUPPORTING INFORMATION

Additional supporting information can be found online in the Supporting Information section at the end of this article.

How to cite this article: Li, M. & Toumi, R. (2025) Can tropical cyclones exist near the Equator?. *Quarterly Journal of the Royal Meteorological Society*, e70014. Available from: https://doi.org/10.1002/qj.70014